ICAS-92-4.3.4

COMPUTATIONAL METHODS APPLIED TO THE AERODYNAMICS OF SPACEPLANES AND LAUNCHERS

J.M. BOUSQUET, R. COLLERCANDY, L. DALA,
A. DEMARGNE, J. OSWALD

Office National d'Etudes et de Recherches Aérospatiales (O.N.E.R.A.)
B.P. 72, 92322 CHATILLON CEDEX (FRANCE)

Abstract

The numerical tools used at ONERA for the aerodynamic analysis of the Hermes spaceplane and its launcher Ariane 5 are presented. They range from panel methods suitable for subsonic to low-transonic flow conditions, to three-dimensional Euler solvers used for supersonic and hypersonic Mach number regimes, the real gas effects being accounted for in the latter case. Applications to different Hermes geometries in the launch phase on top of Ariane 5, as well as in the return flight are performed and compared to wind tunnel results.

Notations :

C_M : Pitching moment coefficient, wind axis

C_N : Normal force coefficient, vehicle axis

C_P : Pressure coefficient

C_Z : Lift coefficient, wind axis

C_X : Drag coefficient, wind axis

M : Mach number

e : energy

u : velocity component along x

v : velocity component along y

w : velocity component along z

X : axial distance

α : angle of attack

γ : specific heat ratio

Θ : angle of keying

μ : doublet strength $\mu = \Phi_e - \Phi_i$

ρ : density

σ : source strength $\sigma = \vec{n} \, (\vec{\nabla}\Phi_e - \vec{\nabla}\Phi_i)$

Φ : potential

Φ_e : outer potential

Φ_i : inner potential

Copyright © 1992 by ICAS and AIAA. All rights reserved.

I. Introduction

Space transportation is likely to be one of the major subjects of aeronautical activity by the end of this century. As the safety of manned and un-manned space missions has to be guaranteed, particular attention has to be paid to the design of space vehicles. This requires sophisticated design tools. Consequently, in parallel to industrial programs (Ariane 5 and Hermes), CNES (French space agency) supports research activities in which ONERA is involved, in particular in aerodynamics.

This paper deals with the numerical tools used at ONERA to analyse the different phases of a spaceplane flight envelope (from the launch to the orbital flight and then from de-orbit to landing). During this flight, all the aerodynamic flow conditions are encountered (subsonic, transonic, supersonic and hypersonic). The analysis of these flow conditions requires the use of different types of flow solvers and associated mesh generators. These will be reviewed in the first part of this paper.

The main aerodynamic concern during launch is the stability in high subsonic / transonic conditions. In this case, the complex interactions between the spaceplane and the launcher may play a key role which must be carefully studied during the design phase of the whole configuration. On such complex geometries the use of rather simple panel methods helps to select the important parameters to be taken into account before wind tunnel validation. For this purpose, the ECOPAN panel method [1] is used and the results are compared to wind tunnel data. This code is also used for the study of the spacecraft landing conditions.

Supersonic computations are undertaken with the FLU3M code [2], which solves the three dimensional Euler equations using an explicit / implicit finite volume method with a MUSCL approach.

The main area of concern during the return flight of the spaceplane is the hypersonic regime. Due to high Mach numbers ($5 \leq M \leq 25$) and to problems in simulating accurately the flight conditions using current wind tunnels, a comprehensive strategy has to be followed. This is done by a validation of the methods at the highest Mach number of current wind tunnels and a projection with numerical techniques into the remaining Mach number range. To

achieve this, ONERA uses the FLU3M code which can take into account real gas effect. The SHABP engineering code is also used for force and moment calculations at these Mach numbers. Both results are compared to wind tunnel data.

The FLU3M method is also used to study the aerodynamic interference of a rear leeward located Reaction Control System, firing in flow conditions which can be simulated in a wind tunnel (Mach 10).

Finally, the range of validity of these different methods is analysed and the areas where research should be increased are reviewed.

II. The numerical methods

ECOPAN Code

The ECOPAN code is used to compute subsonic inviscid flows around three-dimensional bodies such as launchers or complete aircraft [1].

This integral type method is based on the solution of the Laplace equation which is applied to the velocity potential :

$$\Delta \Phi = 0 \quad \text{with} \quad \vec{V} = \vec{\nabla} \Phi \qquad (1)$$

The flow potential induced by the body is defined by the surface distribution of combined doublet-source panels, which are basic solutions of the Laplace equations.

Integral equation for the thick body case :

For a closed surface S, the use of the third Green equation applied to the vector field $\vec{f} = \Phi \vec{\nabla}(1/r) - (\vec{\nabla}\Phi) / r$ gives an integral equation between the potential at a point P and the source and doublet strengths over S :

$$\Phi(P) = \frac{1}{4\pi} \iint_S \mu \vec{n} \vec{\nabla}\left(\frac{1}{r}\right) dS - \frac{1}{4\pi} \iint_S \frac{\sigma}{r} dS + \Phi_\infty(P) \qquad (2)$$

with : $r = | \vec{X}_Q - \vec{X}_P |$ (the point Q belongs to S)

The source and doublet strengths are the unknown variables of this problem. Therefore two boundary conditions are required on the body in order to obtain the solution.

Boundary conditions :

An inner Dirichlet condition is used by the ECOPAN code, (i.e. the potential of the internal virtual flow is prescribed usually $\Phi_i = \Phi_\infty$), in addition to the one on the external normal velocity.

The sources are then equaled to explicit values which depend on external normal velocities. The doublets are also the solution of an integral equation prescribing the condition on the inner potential.

Wakes :

The wing vortex sheets are discretized by wake doublet panels. These panels are equivalent to a vortex lattice which extends infinitely downstream. The vortex circulation is computed by applying a shedding condition (equivalent to a Kutta-Joukowski condition) at the trailing edge of every profile. Different options are available to express this last condition, according to whether or not the trailing edge is thick and whether or not the shedding condition is linearized.

Code extensions :

A Prandtl-Glauert compressibility correction can be used to compute slightly compressible flows.

FLU3M Code

The unsteady 3D Euler equations are written in the conservation law form :

$$W_t + \text{div } \mathbf{f} = 0 \qquad (3)$$

where $W = {}^t (\rho , \rho u , \rho v , \rho w , e)$ is the vector of conservative quantities and f represents the convective fluxes. The system of equations for the unknowns ρ, u, v, w, e is closed by a last equation which depends on the air model, discussed later on.

A finite volume discretization is employed so that the variables W are evaluated at the nodes of a grid with an "ijk" structure. Defining a control volume Ω surrounding each node of the grid, one readily obtains the flux balance formulae for a two time level scheme:

$$\Delta W_{ijk} = -\frac{\Delta t}{\text{vol}(\Omega)} \sum_{l=i,j,k} (F_{l+1/2} - F_{l-1/2}) \qquad (4)$$

where $F_{l+1/2}$ represents the numerical flux at the interface $l + 1/2$.

The explicit part of the scheme uses the 2nd order MUSCL approach associated with van Albada's or minmod limiters and the flux-vector splitting introduced by Van Leer in [3].

In order to accelerate the convergence towards the steady state, an implicit part is added, based on a Steger-Warming type evaluation of the first order terms of the numerical fluxes :

$$F^{impl.}_{l+1/2} = F^{expl.}_{l+1/2} + A^{+}_{l+1/2} \Delta W_l + A^{-}_{l+1/2} \Delta W_{l+1} \qquad (5)$$

where A^+ and A^- represent the exact Jacobians of the upwind flux formulae. An approximate factorization of ADI type leads to block tridiagonal linear systems to be solved in each grid direction. Following, when the flow is supersonic in one direction, the extra-diagonal blocks in that direction are dropped and a two dimensionnal ADI factorization associated with a space marching procedure is used. Convergence is then obtained plane by plane along the supersonic direction.

The boundary treatment on a solid surface and on a matching interface between two computational domains is detailed below.

Solid surface treatment :

At a node on a solid surface, a half control volume is defined which allows the evaluation of both the conservative quantities and the wall fluxes in terms of pressure alone. In

the implicit formulation, the Jacobian of this wall pressure function is taken without any upwinding :

$$F^{impl.}_{wall} = F^{expl.}_{wall} + \frac{\delta F^{impl.}_{wall}}{\delta W} \Delta W_{wall} \qquad (6)$$

Matching interface treatment :

At a boundary node on the interface between two computational domains, a fictitious node in the outward grid direction is defined. At the boundary and fictitious nodes, values are attached for the conservative quantities interpolated in the adjacent domain. The scheme, is then run as for an interior node without any slope correction for the fictitious node. In the implicit formulation a Dirichlet condition is applied which amounts to cancel in (5) the term ΔW_1 or ΔW_{1+1} corresponding to the fictitious node.

Air model :

For Mach numbers below 10, one can assume that the air behaves as a perfect gas, with the pressure related to the energy through the perfect gas equation. In the case of hypersonic flight conditions (re–entry Mach number > 10), the air may be raised up to temperatures at which a perfect gas model can no longer be used. The chemical thermodynamic properties of equilibrium air must be taken into account. The modelisation defined by Srinivisan [4] is used.

SHABP Code

The Douglas Supersonic / Hypersonic Arbitrary Body Program (Mark IV) is a modularized computer program designed to handle a variety of high speed vehicle analysis problems.

The basic methodology consists in modelling the vehicle as a set of flat plates, called elements. On an element by element basis, the local shape and freestream Mach number are used to calculate the pressure. Further details of these methods are given in [5]. The impact methods are those applied to flow facing elements and the shadow methods are applied to those elements facing away from the flow. These methods include the simple Newtonian approach, the small disturbance theory, the shock expansion methods as well as correlations. A combination of methods can be used for very complicated 3D shape (one impact and one shadow per element) after which the pressure contributions from each part of the vehicle can be summed.

In addition to perfect gas inviscid calculations, the SHABP code also performs a viscous analysis . Furthermore, the code takes into account the real gas effects (variable γ) and the free molecular regime.

The SHABP code is highly flexible and cheap to run. This code is provided as an engineering rather than a research tool.

MESH Generation

The starting point of the surface meshes used for ECOPAN and SHABP or the 3D grids for FLU3M, is the CATIA definition of the vehicle geometry. In the case of Hermes, the CATIA definition is provided by Dassault. The Ariane geometry is analytically defined.

For ECOPAN and SHABP calculations, the surface is divided into several domains (nose, wing, winglet, body, booster,...). In each domain, the panels are directly generated with CATIA functions. A typical surface mesh presented in figure 1, represents the Hermes spaceplane atop its launcher Ariane, together with the two lateral boosters. For ECOPAN calculations, a modelization of the wing is necessary. This vortex lattice is analytically defined, while taking into account the shape of the boosters for the Hermes + Ariane configurations (see figure 2).

For Euler computations of the composite Ariane 5 + Hermes 1.0, the surface mesh constructed directly on CATIA is divided in two blocks as seen in figure 3. One block is located between the booster and the main body of Ariane. It extends to the region between the winglet and Hermes fuselage, and then vanishes in a singular line on the leeward wing. The second block surrounds both the surface and the first block. All the external boundaries of these two blocks are also constructed on CATIA. The 3D grid is first built using a 3D transfinite interpolation and then smoothed by a barycentre method. The final wireframe is presented in figure 4.

For the FLU3M computation of Hermes alone, the 3D grid is generated in a slightly different way in order to improve the mesh density in specific areas such as the winglets. The surface mesh is created on a CATIA workstation. Then, this mesh is cut into several 3D domains corresponding to the final computational zones (generally 3 or 4). In each domain, the surface mesh provides a clusterisation of the points on the leading edge while maintaining an iso–indice line on the leading edge and on the leeward root of the wing. At the same time, the external boundary is generated by using simple techniques (generally sphere–cone geometry). The 3D grid is then made of an association of several 2D grids generated with the GRAPE code. They are associated around an axis for the nose region and distributed downstream along the longitudinal axis. The complete 3D grid of Hermes used for the computation is presented in figure 5.

III. Subsonic calculation

Ariane 5 + Hermes 0.0 in launch conditions (M=0.5)

The suface grid of Hermes / Ariane 5 configuration is presented in figure 1 (see II.). It is divided into 15 sub–domains in order to facilitate local analysis of the flow field and local integration of the aerodynamic coefficients. This surface mesh consists of 3312 panels for Hermes 0.0 + adapter to launcher and 3094 panels for the lower part of Ariane 5, which corresponds to half the configuration, used in computations with no sideslip. The surface grid is refined from the trailing edge of Hermes 0.0 to the booster nose of Ariane 5, in order to take precisely into account the interaction between the wake shed from the trailing edge of the wing and the other parts of the launcher, as shown in

figure 2. This type of interaction is of prime interest for the prediction of the longitudinal stability of the launcher. In order to avoid spurious numerical inaccuracies on the border of the wake in the vicinity of the central body a special technique is employed. As illustrated in figure 6, the doublet surface modelling the wing wake is attached to a particular mesh line on the central body and a decoupling condition in the potential is applied. This enables an accurate calculation of the velocities on the central body.

As the most critical phase of the launch is the high–subsonic / transonic range, computations of Hermes 0.0 / Ariane 5 configuration were undertaken at Mach 0.5 for the small angles of attack ($-3° \leq \alpha \leq 3°$) encountered during flight. The pressure distribution over the upper wing surface of Hermes 0.0 / Ariane 5 is presented in figure 7, for two angles of incidence $\alpha = 0°$ and 3°. The compression regions in dark on this figure are located mainly at the nose of the spaceplane, on the cone of the adapter and on the flare of the boosters; they are followed by areas of accelerated flow, at the junction with cylindrical parts. The effect of incidence when going from $\alpha = 0°$ to $\alpha = 3°$ results in a slight extension of these areas, in particular at the winglet leading edge and on the junction of the cone to the cylindrical part of the boosters, which are also slightly influenced by the interaction with the wing wake.

The analysis of the longitudinal coefficients (i.e. the normal force coefficient $C_N(\alpha)$ and the pitching moment coefficient $C_M(\alpha)$), is performed in figure 8, where the ECOPAN code and the wind tunnel test results are compared at Mach 0.5. The computed slope $\partial C_N/\partial\alpha$ is very close to the one found experimentally (i.e. $\partial C_N/\partial\alpha$ is about 0.21, see figure 8a). In the same way, figure 8b shows a good agreement between the calculated and experimental $\partial C_M/\partial\alpha$ ($\partial C_M/\partial\alpha = 0.53$). The prediction of the absolute value of these coefficients is less accurate, especially for the pitching moment, where an average $\Delta C_M = 0.35$ discrepancy between calculation and test is observed in figure 8b.

Figure 9 shows the influence, on the pitching moment coefficient of the Mach number and of the keying angle Θ of Hermes 0.0 on the launcher. As already mentioned, the absolute value of the pitching moment is not accurately predicted by the ECOPAN code. In figure 9a, for the same keying angle $\Theta = 0°$, comparison of Mach 0.5 and Mach 0.8 test results indicates that the compressibility effect on this coefficient is rather small. At this keying angle, the discrepancy between calculation at Mach 0.5 and test data at Mach 0.8 is of the same order of magnitude as the one observed in figure 8b. At the keying angle $\Theta = 2°$ (figure 9b), the Mach 0.8 wind tunnel pitching moment coefficient is compared to the computed Mach 0.5 coefficient. The increase of the keying angle results in a increase of the pitching moment with almost no change in the slope of the curves. This effect is correctly accounted for by the ECOPAN code which predicts $\Delta C_M = 0.4$ due to the keying angle (figure 9a and 9b), while the difference between $\Theta = 0°$ and $\Theta = 2°$ is $\Delta C_M = 0.5$ for the tests.

Hermes 1.0 Landing (M=0.2)

In the final part of the flight, the aerodynamic characteristics of the Hermes spaceplane are computed by the ECOPAN code.

The surface mesh used in these computations is of the same type as the one presented in the launch configuration, with only Hermes modelled by source–doublet type panels. Typical grid density is approximately 2700 panels for the half configuration used in the longitudinal computations where symmetry conditions are applied. The wake of the wing and winglet is modelled by panels of doublet type. At the rear of the fuselage, either a contoured fairing or a cylindrical sting is disposed in order to simulate the base flow not accounted for in the purely inviscid calculation.

The evolution of the computed lift coefficient with angle of attack is presented in figure 10, for two different versions of the Hermes spaceplane (Hermes 0.0 and Hermes 1.0) at Mach 0.2. The comparison with experimental results shows a good agreement on Hermes 0.0 for angles of attack up to $\alpha = 10°$, where the experimental curves exhibit an increase of the lift coefficient derivative, typical of vortex lift on highly swept delta wings, and not accounted for in the ECOPAN calculation. In the case of Hermes 1.0, the agreement between calculation and test is slightly less satisfactory, with a slight overestimation of the zero lift coefficient ($\Delta C_Z = 0.01$ for $\alpha = 0°$), but with a correct evaluation of the slope $\partial C_Z/\partial\alpha$ as long as the vortex lift increment is not significant ($\alpha < 12°$).

The longitudinal stability predictions are not as accurate, as illustrated in figure 11. Clearly, the pitching moment C_M computed by the ECOPAN code for both Hermes 0.0 and Hermes 1.0, do not match exactly experimental value. It should be noted that the two versions of Hermes differ essentially in the camber of the airfoils and the location of the center of gravity.

Nevertheless, the difference of C_M between the two configurations is approximately constant for $C_Z \leq 0.4$ with a slight overestimation in the calculations (ΔC_M=0.024 in calculation and C_M=0.02 in test). The difference of slope $\partial C_M/\partial C_Z$ (static instability) between the two configurations is small both in the calculations and in tests. Additionally, the Hermes 1.0 configuration appears more difficult to compute (as was the case for the lift coefficient), probably due to the geometrical differences with Hermes 0.0 in the rear part of the fuselage, where the body–flap extends further behind the trailing edge of the elevons.

As a conclusion, the ECOPAN code is appropriate to subsonic computations of spaceplanes. Although the computed absolute values of lift and pitching moment coefficients are slightly different from experimental values, the trends computed by this code are accurate. It is therefore well suited to comparative studies of different configurations and sensitivity studies.

IV. Supersonic calculation

Ariane 5 + Hermes 1.0 to Launch (M=1.47)

The supersonic Euler computation of the composite Ariane 5 + Hermes 1.0 is undertaken with the FLU3M code by using the time marching option. The wireframe, whose generation is defined in II. and figures 3 and 4, has 137 x 54 x 35 = 258 930 nodes in the wide block and 92 x 13 x 11 = 13 156 nodes in the second one. The keying angle between Hermes and Ariane is set to $\Theta = -2°$. The three angles of attack 0°, 2° and 5° were chosen for this Mach 1.47 perfect gas computation.

In figure 12, the Mach number contours in the symmetry plane are presented, for the case $\alpha = 0°$. One can notice the sharp description of the shock structures captured in the solution, which are followed by subsonic zones in the nose region, on the windshield and on the lower part of the conical transition of Hermes to Ariane central body. The expansion zones are also well captured on the top of the canopy and at the end of the conical transition to Ariane central body. Additionally one can notice downstream the trace of the shock coming from the booster noses. At the rear part of the central body a subsonic zone with recirculating flow has been captured in the solution. This shows the robustness of the method, but should not be considered as an accurate prediction of the recirculation zone since viscous effects are not accounted for in the Euler method. The Iso-Mach number lines in the mesh section, (figure 13), show a subsonic region in the leeward side of the winglet and the generation of a shock around the winglet for the angle of attack $\alpha = 5°$.

The pressure coefficient distribution corresponding to the leeward and windward line in the symmetry plane for the three angles of attack, are plotted in figure 14. The shocks or expansions visible on the iso-Mach number representations are once again observed. The effect of the angle of attack on Hermes and on Ariane, is clear. The pressure is increased on the winward side while decreased on the leeward side. These effects contribute to the increase of lift.

These computation results are currently used to analyse the Hermes + Ariane behaviour in supersonic flow. They will be compared to wind tunnel test results when available, to enforce the validation of the FLU3M method in these conditions.

V. Hypersonic calculation

Hermes 1.0 De-orbiting (M=10 and M=25)

The computation of the inviscid flow around Hermes 1.0 at Mach 10 is carried out with the FLU3M code with a perfect gas model, which is consistent with simulations in ONERA wind tunnels R3 Chalais or S4 Modane. At Mach 25, real gas effects are taken into account in FLU3M using tabulated chemical thermodynamic properties. In this case, no wind tunnel test results are available to compare with. The computations are performed at an angle of attack of 30° and with no sideslip. The mesh generation for half a plane is described in II. The first block (43x34x40 nodes) is calculated using the time marching option of FLU3M in order to treat correctly the subsonic zone around the nose of Hermes. In the aft blocks (61x46x37 and 121x46x23 nodes), where the normal Mach number along the spaceplane direction is always supersonic, the faster space marching option of FLU3M is used.

The Mach number distribution in the plane of symmetry (figure 15) shows that the bow shock is sharply captured. Comparison of Mach 10 and Mach 25 solutions indicates that the bow shock on the windward side is closer to the surface due to real gas effects. The same effect can be seen on the leeward side. The canopy shock, which is clear for Mach 10, seems to disappear at Mach 25. The Mach number contours at cross section X = 12.9m are presented in figure 16 . Once again, one can notice that the bow shock is closer to the windward side for the Mach 25 case. Additionally, cross-flow shocks are present on the top of the Hermes fuselage and over the wing with a better resolution at Mach 10 than at Mach 25. The pressure coefficients, in the same cross section, for the two Mach numbers are presented in figure 17. The sharply described bow shock is closer to the lower side and to the winglet at Mach 10 than at Mach 25. One can also notice the winglet shock near the winglet leading edge, which is stronger for the real equilibrium air calculation. In both cases, there are low pressure levels on the leeward side, which may lead to flow solutions probably at the limit of validity of Euler equations, in particular in the wing / winglet junction region.

The computed global forces and moments (M = 6.4 ; 10 ; 15 ; 25) are compared to wind tunnel results in R3 Chalais at Mach 10 and S4 Modane at Mach 6.4, in figure 18. The SHABP results are also presented.

The discrepancies on drag coefficients between FLU3M, SHABP and wind-tunnel results are small (figure 18a). For this angle of attack α = 30°, in the case of perfect gas (Mach 6.4 or Mach 10), the greatest difference between FLU3M and wind tunnel results is on the pitching moment, corresponding approximately to 1° of pitch control surface deflection. The real gas effect, quantified between Mach 10 and Mach 25, consists in a decrease of $\Delta CZ = -0.01$ for lift coefficient (figure 18b) whereas the pitching moment increases by $\Delta CM=0.0045$ (figure 18c). This modification of the aerodynamic behaviour is essentially due to the closer proximity of the bow shock to the windward side at Mach 25 which increases the pitch up tendancy. The SHABP prediction of real gas effects gives the same trend, but with a lower amplitude ($\Delta CZ = -0.006$ and $\Delta CM = 0.002$)

Overall, the FLU3M code has been seen to provide realistic values for the global coefficients which are used in flight mechanics studies. The flow fields computed by FLU3M are also the starting point of the boundary layer and heat flux calculations.

R.C.S. (M=10)

The aim of this preliminary study was to simulate numerically a Reaction Control System (R.C.S.) thruster

operating under re–entry conditions, in view of predicting its performance and control effectiveness.

A pitch–up thruster was chosen for this first computation, on the basis that the aerodynamic interaction would be slight and that there would be no impingment of the jet plume with the surface of Hermes. In order to avoid the use of a real gas model, the freestream Mach number was chosen at 10, corresponding to an altitude of about 52 km on the re–entry trajectory. In addition, these flow conditions would be easily simulated in hypersonic wind tunnels.

The calculation was performed using the FLU3M Euler code, together with a time marching procedure. A refined grid (60x94x50 points) was used in the sub–domain containing the nozzle. In this way, 4x4 points were positioned in the nozzle exit.

The resulting Mach contours are shown in figures 19 and 20. The flow in a longitudinal plane through the jet (figure 19) clearly shows the presence of a detached shock upstream of the jet, followed by the jet boundaries and finally, a region of recirculating flow behind the plume. Note that since viscous effects have not been accounted for, there is no boundary layer separation and no separation shock. The Mach contours in a cross–section through the jet are shown in figure 20. Comparison with those in the absence of jet shows that the shock structure from the jet interacts with the fuselage crossflow shock and tends to push it towards the wing. Apart from this, the influence of the jet on the remainder of the flow is slight. The computed curves of cumulated pitching moment , with and without jet, are given in figure 21. The relative increase in pitching moment was found to be about 10 %, which corresponds at Mach 10 to a control surface deflection of around 0.6°. The amount of aerodynamic interaction was evaluated using the amplification factor, which is the ratio of reaction and interaction forces to the vacuum thrust of the jet. This factor was estimated to be about 1.9, which is relatively slight but consistent with the position of the thruster on the vehicle.

Finally, this preliminary computation showed that numerical simulation provided satisfactory inviscid predictions of the flowfield and forces induced by an RCS jet, fired from Hermes during re–entry.

VI. Conclusion

The numerical tools available at ONERA for the study of the aerodynamics of complete 3D spaceplanes and their launchers have been reviewed.

In subsonic flow, the ECOPAN panel code is a reliable tool to study complex geometries as Hermes on top of its launcher Ariane 5, including the effect of the interaction of wing wakes with boosters. For the more sensitive pitching moment predictions, this method has to be used on a comparative basis; the absolute values may differ from experimental results but the derivatives of this coefficient with respect to angle of attack or shape modifications are well accounted for.

In supersonic and hypersonic flow, the FLU3M Euler code is a robust and efficient method, which allows a sharp description of shock structures. The prediction of the aerodynamic coefficients is in reasonable agreement with wind tunnel results, and with the simpler SHABP code results. For higher Mach numbers, the account of real gas effects enables the detailed study of severe re–entry conditions of the Hermes spaceplane. Although not presented here, the cross–checking with other code results has already enforced the confidence in the method for the prediction of hypersonic flows.

These aerodynamic results are currently used as inputs for thermal studies by means of boundary layer calculations.

Future activities will cover transonic regimes [6], RCS jets and sideslip conditions at hypersonic regimes,and in general will take larger account of viscous effects in the aerodynamic prediction.

References :

[1] Roggero F., Larguier R. : "Aerodynamic calculation of complex three–dimensional configurations" 17th ICAS Stockholm (Sweden), Paper No 90–6.4.3.

[2] Guillen P., Borrel M. : "Hypersonic delta wing flow calculations using a multidomain MUSCL Euler solver" Workshop Hypersonic INRIA Sophia Antipolis, Antibes, January 22–26, 1990.

[3] Van Leer B. : "Flux Vector Splitting of the Euler Equation" Lecture notes in Physics, Vol 170, 1982 p. 507 –512.

[4] Srinivisan S., Tannehill J.C., Weilmuenster K.J. : "Simplified Curve fits for the Thermodynamic Properties of Equilibrium Air" NASA RP 1181 1987.

[5] Gentry A.E. et al : "The Mark IV Supersonic / Hypersonic Arbitrary Body Program" Vol I&II AD–778443–444 November 1973.

[6] Collercandy R., : "An improved approach for the computation of transonic / supersonic flows with application to aerospace configurations " AIAA paper Palo Alto 92–2613, (USA).

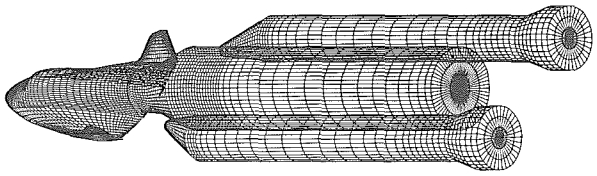

Figure 1 : Surface mesh of Ariane 5 / Hermes 0.0 configuration for ECOPAN computation.

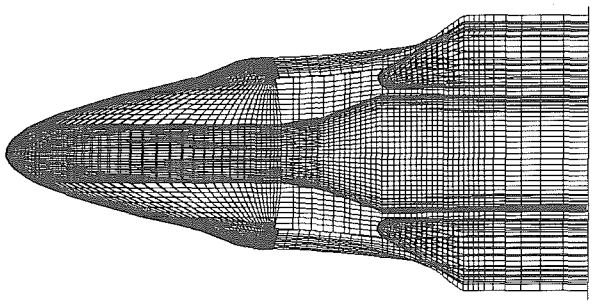

Figure 2 : Vortex lattice shed from the trailing edge of Hermes 0.0, in the booster area of Ariane 5.

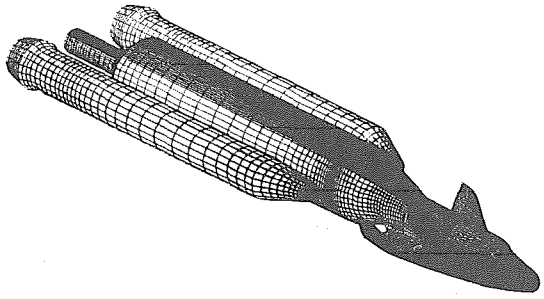

Figure 3 : Surface mesh of Ariane 5 / Hermes 1.0 configuration. Two block structure for Euler computation.

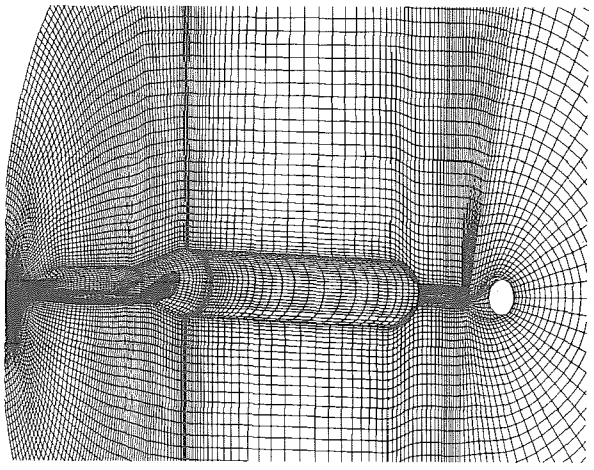

Figure 4 : 3D Euler grid around the Ariane 5 / Hermes 1.0 configuration (booster not represented).

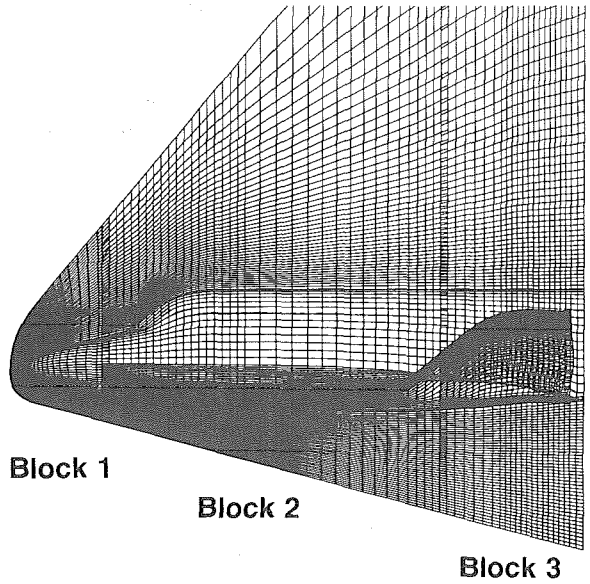

Figure 5 : Three block structure of the Euler grid around Hermes 1.0.

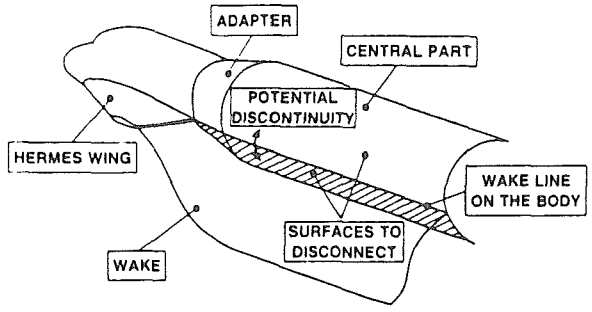

Figure 6 : Schematic representation of the junction between the Hermes wake and the central body (ECOPAN computation).

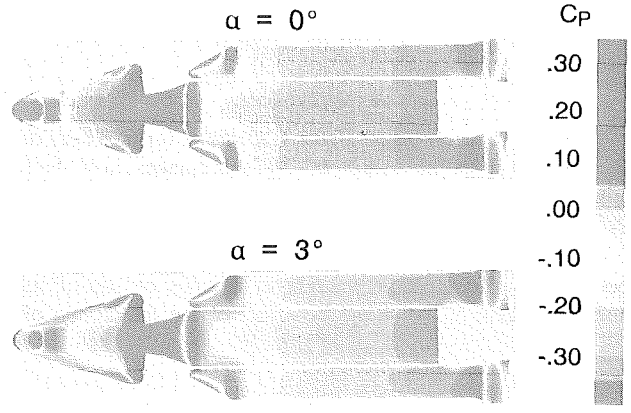

Figure 7 : ECOPAN computed pressure field on the Ariane 5 / Hermes 0.0 configuration (leeward side; M=0.5; Θ=0°).

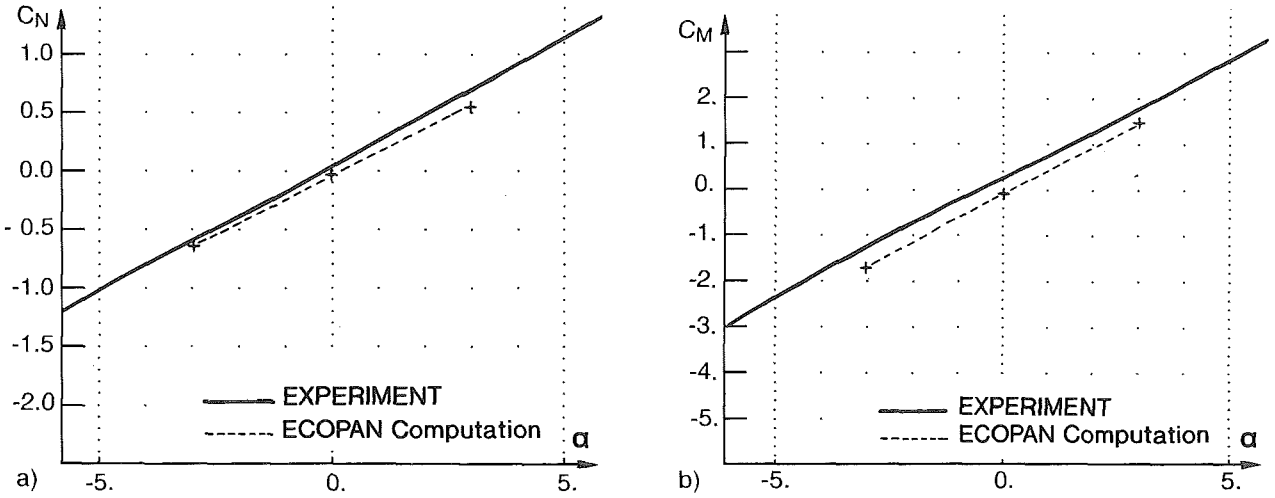

Figure 8 : Ariane 5 / Hermes 0.0 : Normal force and pitching moment coefficients versus angle of attack. Comparison of ECOPAN results with wind tunnel data (M=0.5 ; Θ=0°).

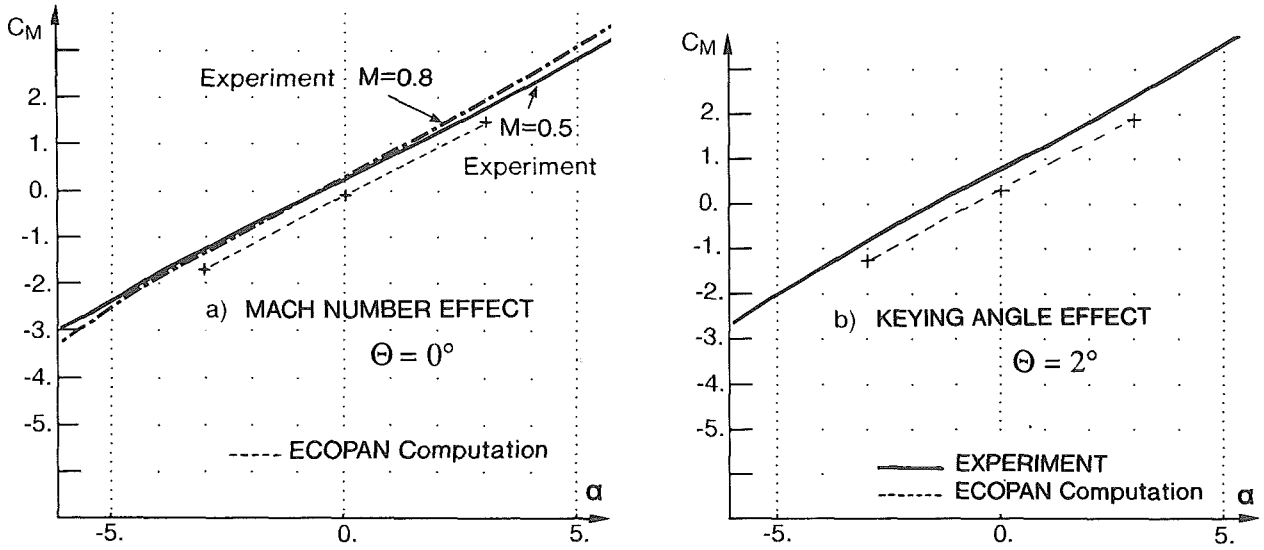

Figure 9 : Ariane 5 / Hermes 0.0 : Pitching moment coefficient versus angle of attack. Comparison of ECOPAN results with wind tunnel data.

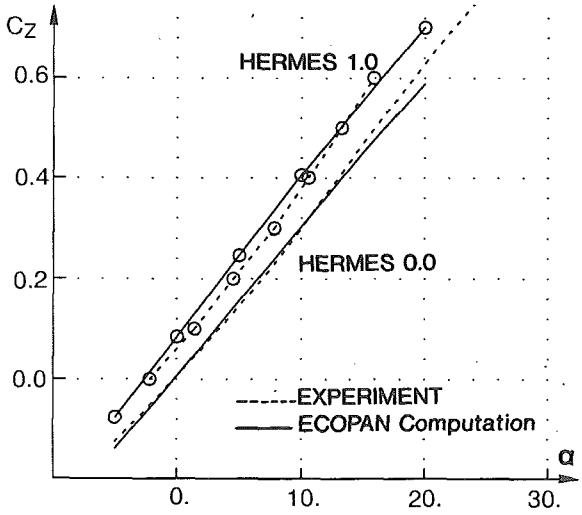

Figure 10 : Hermes 0.0 and 1.0 : Lift coefficient versus angle of attack. Comparison of ECOPAN results with wind tunnel data (M=0.2).

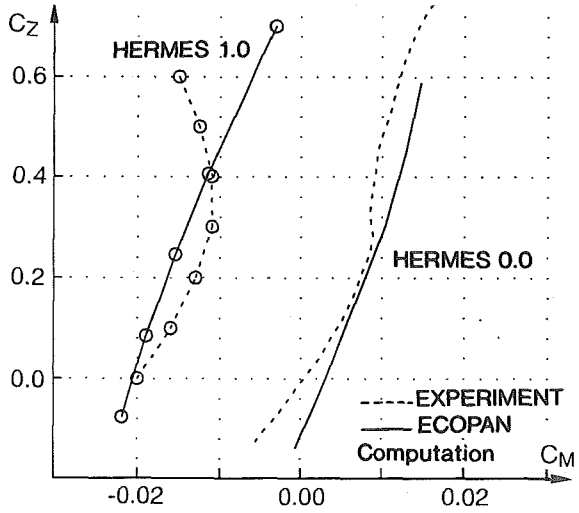

Figure 11 : Hermes 0.0 and 1.0 : Lift coefficient versus pitching moment coefficient. Comparison of ECOPAN results with wind tunnel data (M=0.2).

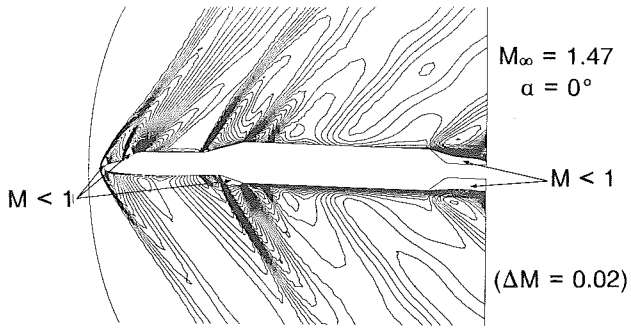

Figure 12 : FLU3M computation : Mach number contours in the plane of symmetry for the Ariane 5 / Hermes 1.0 configuration.

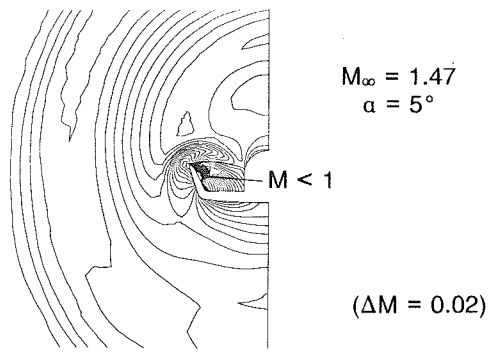

Figure 13 : FLU3M computation : Mach number contours in a grid cross section for the Ariane 5 / Hermes 1.0 configuration.

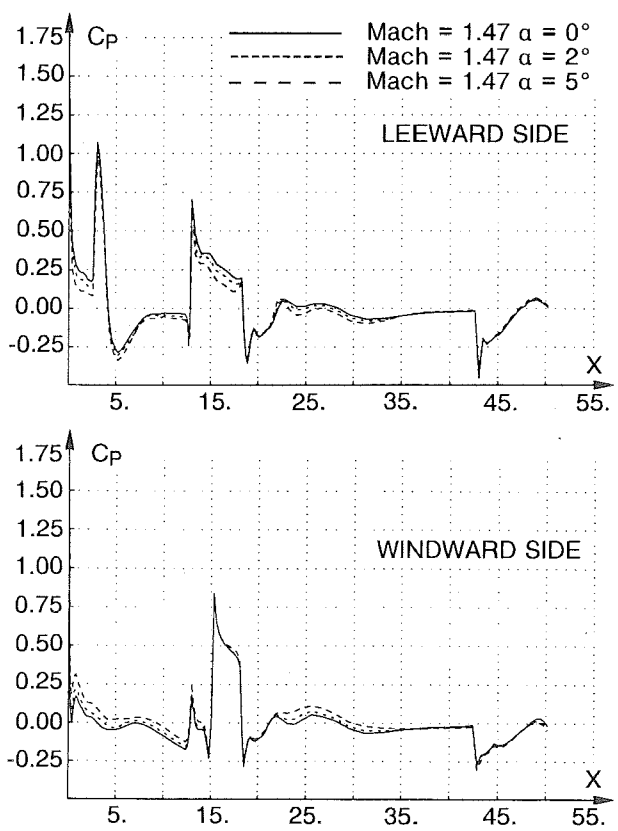

Figure 14 : FLU3M computation : Pressure distribution in the plane of symmetry for the Ariane 5 / Hermes 1.0 configuration.

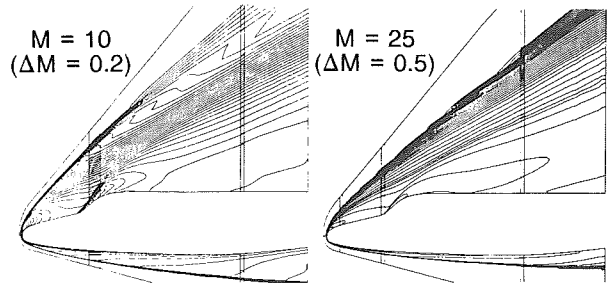

Figure 15 : Hermes 1.0 : FLU3M Mach number contours in the plane of symmetry (α=30°).

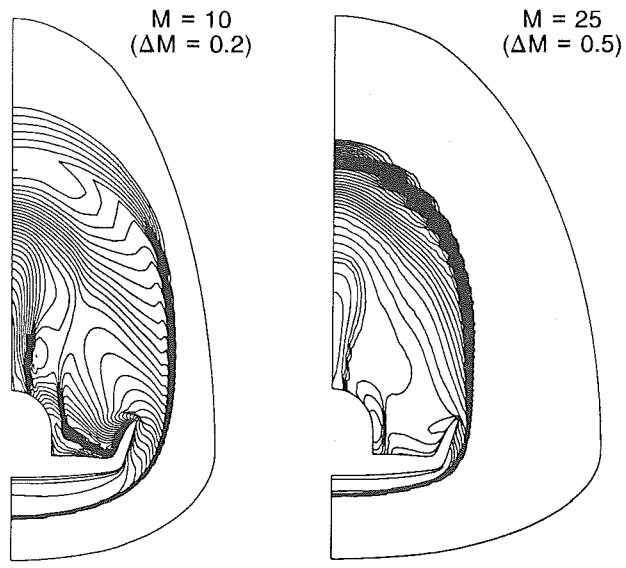

Figure 16 : Hermes 1.0 : FLU3M Mach number contours in a cross section x=12.9m (α=30°).

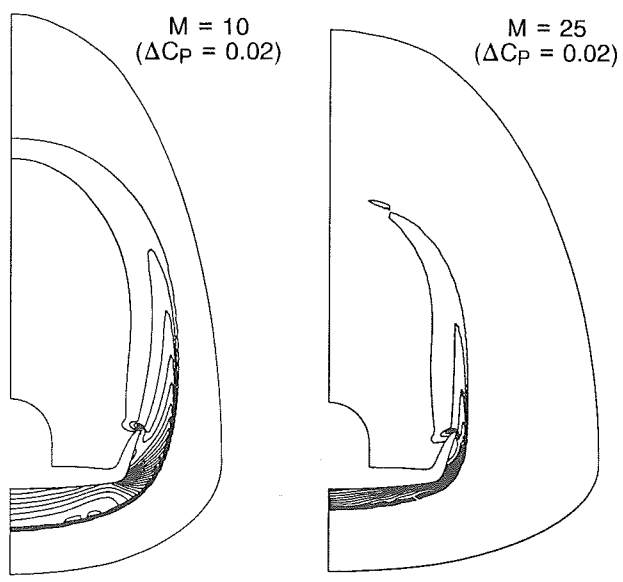

Figure 17 : Hermes 1.0 : FLU3M pressure contours in a cross section x=12.9m (α=30°).

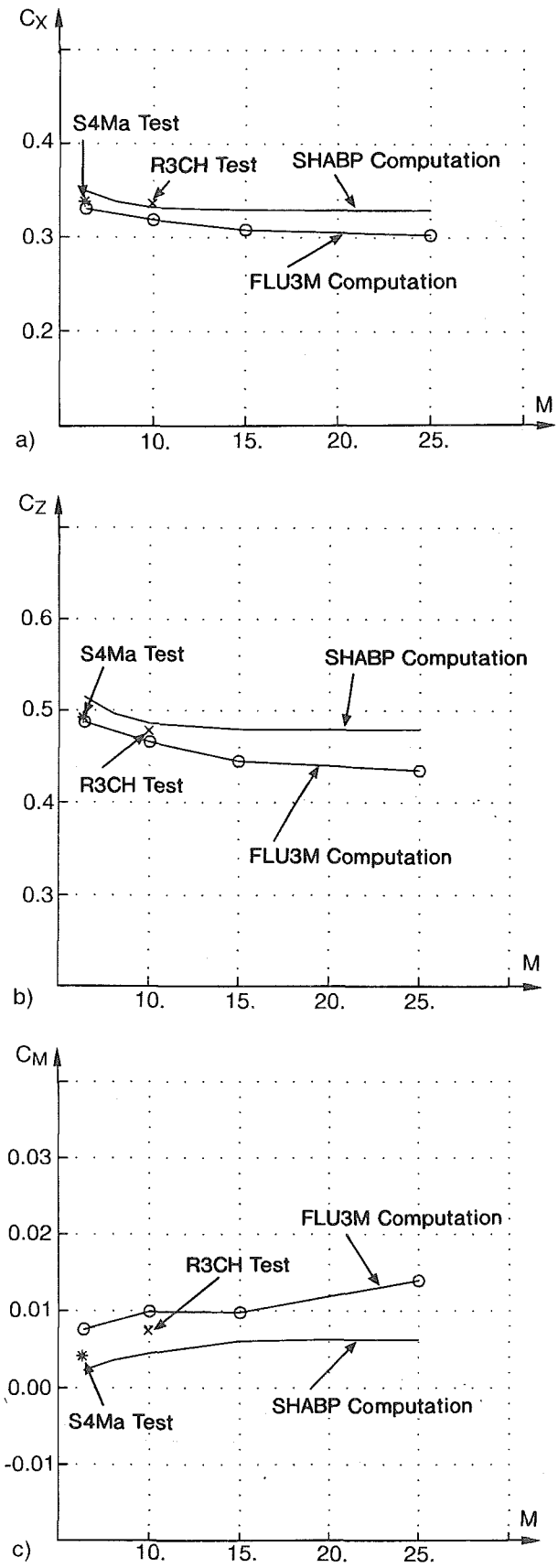

Figure 18 : Hermes 1.0 : Comparison of FLU3M drag, lift and pitching moment coefficients with SHABP computations and wind tunnel data, at different Mach numbers.

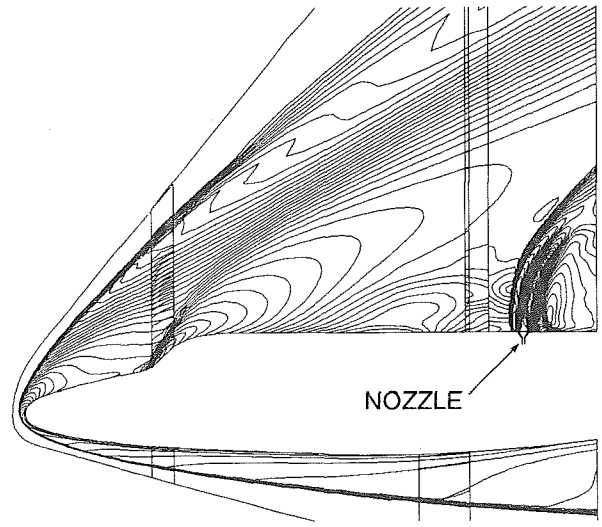

Figure 19 : Hermes 1.0 : FLU3M Mach number contours in a longitudinal plane through the RCS jet (M=10 α=30° ΔM=0.2).

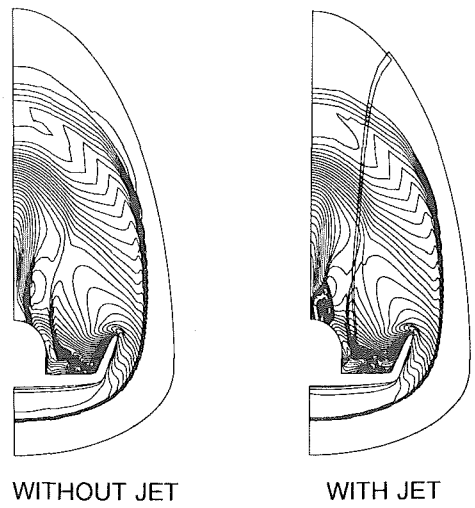

Figure 20 : Hermes 1.0 : Comparison of FLU3M Mach number contours in a cross section containing the RCS jet (M=10 α=30° ΔM=0.2).

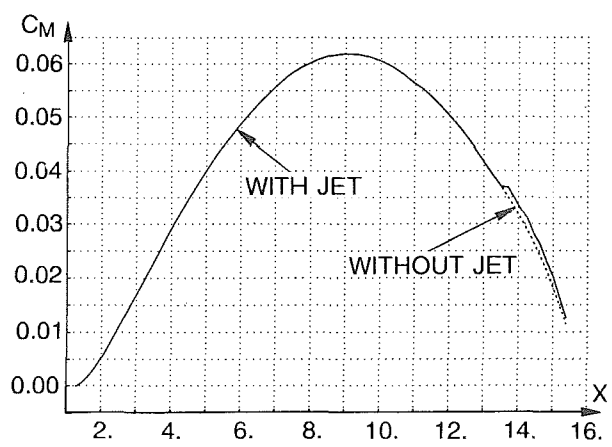

Figure 21 : Hermes 1.0 : Effect of the RCS jet on the FLU3M cumulated pitching moment (M=10 α=30°).